Low-Power Measurement of Contact Impedance in Dry Electrocardiography

M. J. BURKE, C. MOLLOY,
Dept. of Electronic and Electrical Engineering
University of Dublin, Trinity College,
College Green, Dublin2.
IRELAND
mburke@tcd.ie comolloy@tcd.ie http://www.tcd.ie/eleceng/

H. FOSSAN
Laerdal Medical AS
PO Box 337, Tanke Svilandsgate 30, N-4002, Stavanger.
NORWAY
helge.fossan@laerdal.no http://www.laerdal.com/

Abstract: - This paper reports the design of an improved circuit for monitoring the quality of contact of un-gelled electrodes with a patient's skin in the measurement of the ECG. The circuit is intended to be incorporated into a monitor used prior to and during childbirth to measure the mother's heart rate. The revised design uses commercially available low-power technology to implement the circuit with a reduction in the power consumption by a factor of more than 40 over a previous design [13,14]. The circuit measures electrode contact impedance and activates a visual alarm when the contact impedance of either electrode rises above 100kΩ. The impedance is measured using a signal injected through the electrodes at a frequency of 5kHz. The resulting signal present at the amplifier input at this frequency is then extracted and processed before threshold detection of the signal level which is used to indicate whether or not the quality of contact with the electrodes is acceptable for the purposes of heart rate measurement. The circuit operates at a current of 700μA drawn from a 3.3V supply which gives a power consumption of 25mW.

Key-Words: - Electrode impedance, Un-gelled electrodes, Heart rate monitoring, ECG amplifier.

1 Introduction

The Safer Births Program [1], sponsored by the Norwegian Research Council as part of a larger World Health Organization initiative [2], is an action plan aimed at eliminating preventable deaths of infants at birth, with particular focus on developing countries. Many maternity units in such countries are understaffed and often rely on midwives and nurses to contend with complications that arise around birth, without access to the medical assistance or equipment needed to deal with them. Few places have sufficient equipment for fetal monitoring such that fetuses in distress may not be adequately attended, adding to the burden of birth asphyxia and stillbirth. Many of the infants born may not be breathing correctly, or have pulses which are difficult to detect manually. On occasions these infants can be misclassified as stillborn when, in fact, their hearts have not stopped functioning and they could be resuscitated with the help of suitable equipment. Laerdal Medical AS is a Norwegian company that manufactures monitoring and resuscitation equipment for the scenarios described above. One such product is the Moyo unit shown in Fig.1.

Fig.1 The handheld Moyo unit

This unit is a fetal heart rate monitor which uses an ultrasonic transducer placed on the mother's abdomen to detect the infant's heart beat and indicates the fetal heart rate on a LCD display. One common problem with ultrasonic heart rate monitors is that when the infant's heart beat is difficult to detect the transducer often picks up the mother's heart rate in error [3]. In order to overcome this problem the Moyo unit incorporates an ECG amplifier and circuitry that measures the mother's heart rate from her ECG and indicates this separately on the LCD display. The Moyo unit is held by the mother giving birth with her fingers on the stainless steel electrodes of the unit which then measures and displays her heart rate. The values of the two heart rates can then be compared by the midwife or maternity staff and used to discern whether the ultrasonic transducer is measuring the infant's heart rate reliably or the mother's heart rate in error. To this end it was decided to implement a mechanism in the Moyo unit which would verify that the mother's ECG was picked up reliably by the stainless steel un-gelled electrodes. This is done by measuring the contact impedance of the skin-electrode interface at both electrodes of the Mojo unit and detecting when the mother has pressed her fingers onto the electrodes. The circuit reported in this paper measures the electrode contact impedance and activates a visual alarm when the contact of either electrode is unsatisfactory. An earlier version of the circuit is redesigned to consume 46 times less power.

2 Background

2.1 Existing ECG amplifier

The schematic diagram of the front-end ECG amplifier currently in use in the Moyo unit is shown in Fig.2. This is a three-stage instrumentation ECG amplifier adapted from an earlier design by Burke & Gleeson [4, 5] and later improved by Assambo & Burke [6 - 9]. The 46dB of differential gain is split primarily between the first stage with 14.4dB and the second stage with 25.6dB, while the third stage provides 6dB of the gain with differential-to-single-ended conversion. The input stage provides high differential-mode and common-mode impedances of 100MΩ in order to preserve adequate common-mode-rejection-ratio (CMRR) when interfacing with high-impedance dry electrodes. The amplifier operates from a single 3.3V supply rail and the input stages are biased to a mid-rail voltage of 1.65V using a separate dc-to-dc converter chip not shown in the schematic. The ESD protection and r.f. suppression elements are also omitted for clarity.

2.2 Electrodes

The electrodes used in the Moyo unit shown in Fig.1 are made of stainless steel with a blasted matt-finish surface, as these can easily be disinfected before use

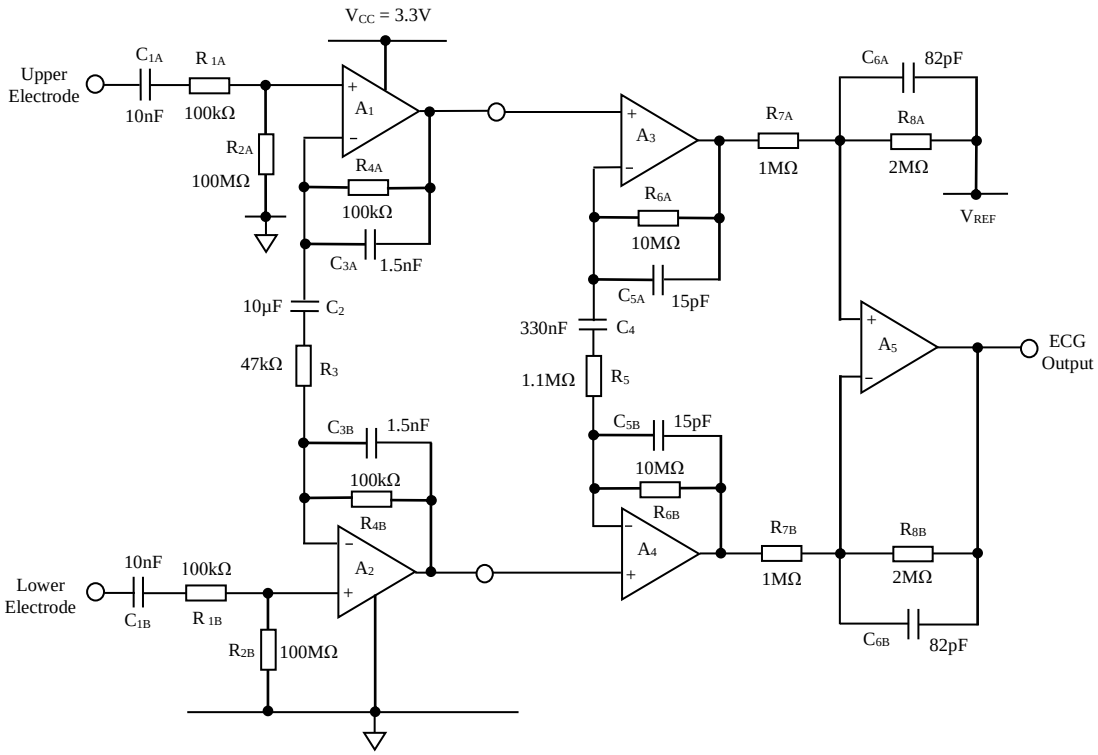

Fig.2 Schematic diagram of existing ECG amplifier

with an alcohol wipe. Electrical contact is made with the electrodes by the mother gripping the unit in both hands with her fingers placed on the electrode surfaces as shown. The firmness of the mother's grip determines the contact pressure. In order to obtain an indication of the contact impedance of these electrodes a method formerly reported by Baba & Burke [10, 11] was used to characterize the electrodes. The current source shown in Fig. 3 was used to inject a minute current of 2μA through the electrodes held by the user. The current was activated and then deactivated via the relay for stable periods of 20 – 50s. A 10kHz sinewave signal was also used to allow the high-frequency purely resistive components to be evaluated. A program in MatLab (MathWorks Inc.) was then used to fit a double time-constant C-R model shown in Fig.4 to the recorded voltage waveforms and to determine the values of the individual components of the model.

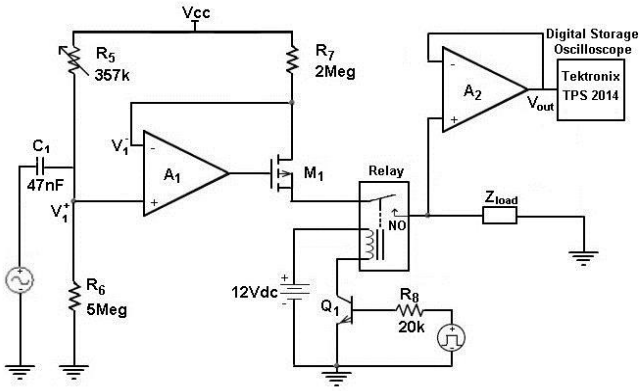

Fig 3 Electrode impedance measurement circuit

Measurements were made on 20 subjects to get an initial idea of the scale and variation of electrode contact impedance to be expected. The subjects were divided into groups of four, including two male and two female, having different ethnic origins, namely: European (Irish), African, Chinese, Latin (Brazilian and Portuguese) and Indian. Only the passive components of the model were of interest in this instance and the dc polarization potentials were not measured. The ranges of values obtained for each component of the model are listed in Table 1. Plots of the magnitude and phase as functions of frequency of the contact impedance of the stainless steel electrodes used in the Moyo unit are shown in Figs. 5(a) - 5(e) for each of the ethnic groups. Plots are shown for a light thumb-grip on the electrodes and for the falling phase of the injected current. These combinations are chosen as they are representative of the highest values of contact impedance measured in each group.

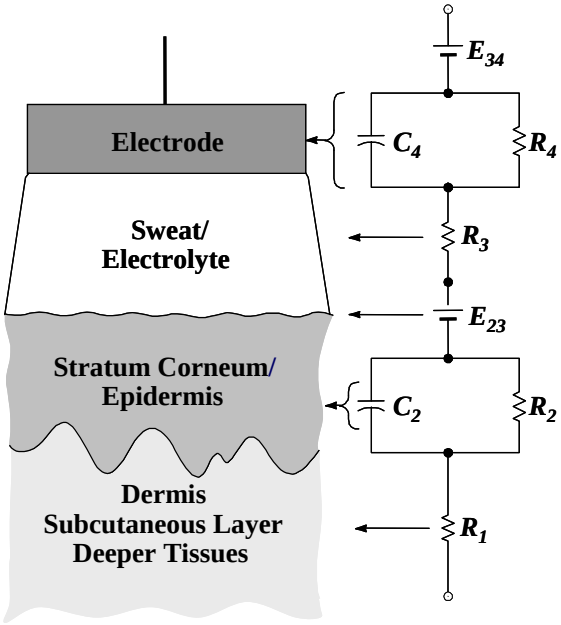

Fig.4. Equivalent electrical model of ECG electrode

Table 1. Range of values of the model elements

Element	Minimum	Maximum	Unit
$R_1 + R_3$	2.0	5.0	kΩ
R_2	23.2	267	kΩ
C_2	1.60	878	μF
R_4	36.0	380	kΩ
C_4	0.47	55.5	μF
τ_2	0.26	58.8	s
τ_4	0.13	8.62	s

It can be seen that the impedance varies considerably within the frequency range of the ECG signal. The magnitude falls off abruptly at very low frequencies below 1Hz and then gradually lowers in steps within the ECG frequency range. Finally, it levels out at purely resistive values above 10kHz. There is also significant variation in the phase of the contact impedance throughout the same frequency range. The effects of these variations can be minimized by making the input impedance of the recording amplifier very high.

It can also be observed that the magnitude of the impedance at its limiting high-frequency value is considerably less than 100kΩ, and in most cases is less than 50kΩ. This value is reached at a frequency of 1 - 10kHz. It is this frequency range that will be used for measurement of the contact impedance. It should be noted that the values of the contact impedance in this frequency range are much lower than the input common-mode resistance of the amplifier. This indicates that the signal levels involved in measuring the contact impedance of such electrodes are likely to be quite low.

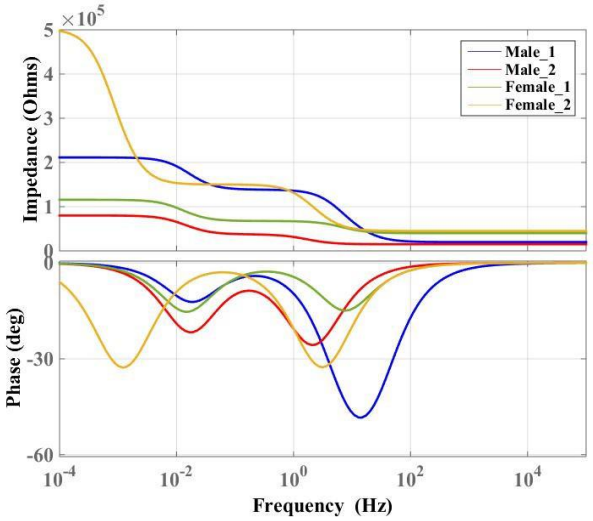

Fig.5(a) Electrode impedance: African subjects

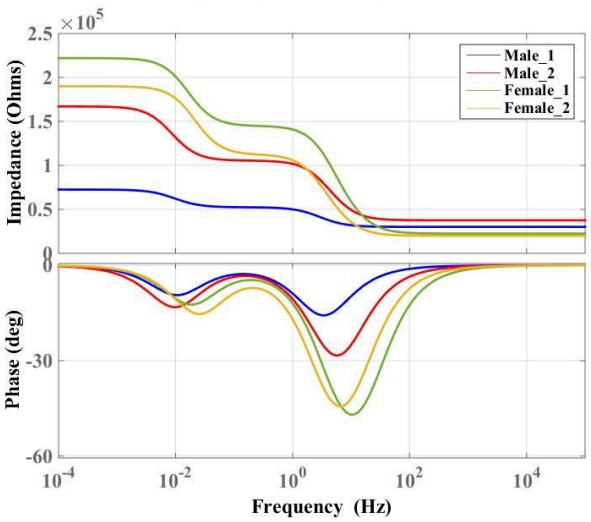

Fig.5(b) Electrode impedance: Irish subjects

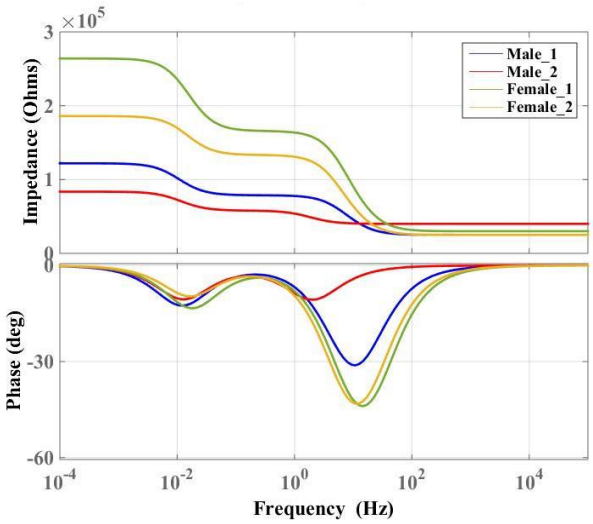

Fig.5(c) Electrode impedance: Indian subjects

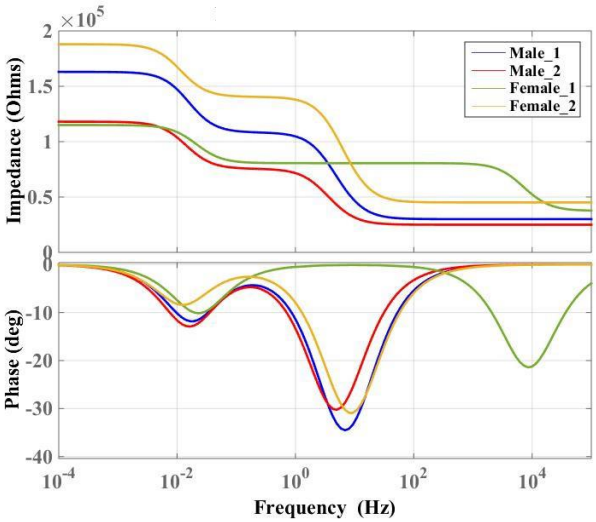

Fig.5(e) Electrode impedance: Latin subjects

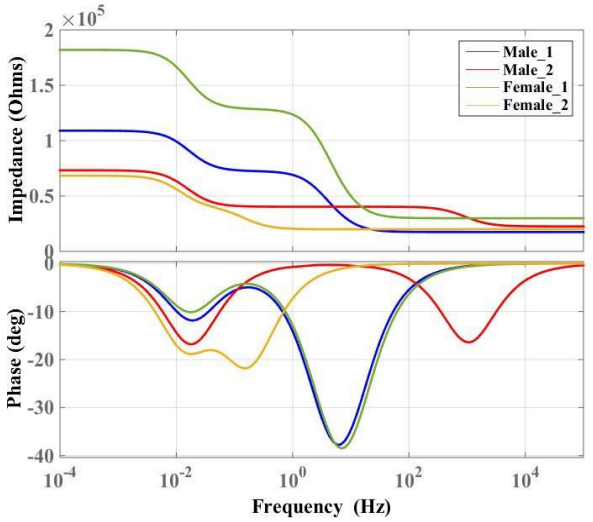

Fig.5(d) Electrode impedance: Chinese subjects

3 System design

3.1 Measurement methodology

A block diagram of the electrode contact monitoring system and its placement in relation to the ECG amplifier is shown in Fig.6. An oscillator and bandpass filter are used to provide a sinusoidal source signal at a frequency of 5kHz with an amplitude of 1.35V peak. Normally one would like the frequency of contact measurement to be much higher than the bandwidth of the ECG signal. However, the parasitic input capacitance of the operational amplifiers as well as the rf suppression capacitors at the input of the amplifier cause a significant shunting effect at higher frequencies. Consequently a frequency of 5kHz was chosen to avoid this shunting effect, while also maintaining

the measurement frequency at least a decade above the ECG band. Following this, the excitation sinewave is then buffered in both an inverting and a non-inverting amplifier to provide antiphase source signals. These signals are then fed through the common-mode input resistors of the ECG amplifier, R_{2A} and R_{2B}, to the electrode impedances, Z_{EA} and Z_{EB}. This method of feeding the contact monitoring signal to the electrodes preserves the high common-mode impedance of the amplifier input and consequently the CMRR. The first stage of the ECG amplifier is also used to provide initial gain for the contact monitoring signal. Band-pass filters centred at 5kHz are used to extract the contact monitoring signal at the differential outputs of the first stage of the ECG amplifier. The signals at the output of the upper and lower band-pass filters are then fed into half-wave rectifiers on each side to provide envelope detection of the amplified signals and generate steady-state signals that give an indication of the magnitude of the contact impedance of each electrode with the skin. This means that a definitive signal is available to the following pair of threshold detectors for decision making on the quality of electrode contact. A threshold detector output will change state when the corresponding electrode contact impedance has exceeded the acceptable level and is then used to drive the corresponding LED to provide a visual alarm indicating this condition.

3.2 Signal generation and injection

A schematic diagram of the circuit used to generate the source signal needed and to inject it through the electrodes is shown in Fig.7. An astable multivibrator is formed around the op-amp A_6, which generates a square-wave signal at 5kHz at the amplitude of the supply voltage of 3.3V. A more suitably shaped waveform is obtained by taking the oscillator output signal from the top of the capacitor C_7, where an exponential charging/discharging voltage is present, rather than from the output of the op-amp itself. This signal has a higher fundamental component present in its frequency spectrum and consequently provides a more sinewave-like signal prior to filtering. This signal is buffered by op-amp A_7 to avoid loading the charging network of the oscillator and is then filtered in the multiple-feedback band-pass filter built around op-amp A_8 to give an almost pure sinewave as the source signal for electrode contact measurement. This provides a sinewave with an amplitude of 1.35V peak. The sinewave is then passed through two buffer amplifiers, a non-inverting unity-gain stage built around op-amp A_9 and a unity-gain inverting stage built around op-amp A_{10}, which also have mid-supply rail bias voltages applied to allow single-polarity supply operation. The in-phase component is fed to the upper electrode point via the upper-channel common-mode input resistor R_{2A}. The inverted component is fed to the lower electrode contact point via the lower-channel common-mode resistor R_{2B}. Each of these common-mode resistors has a 1pF capacitor in parallel with it in order to lower the impedance at 5kHz to 24MΩ while preserving the resistance at 100MΩ within the ECG signal bandwidth. This allows a higher 5kHz measurement signal level to be obtained at the input of the ECG amplifier. The use of antiphase components allows the signal developed on the patient's body to be kept close to zero. The levels of the 5kHz signals developed at the input terminals of the ECG amplifier are those developed across the contact impedances of each electrode namely, Z_{EA}

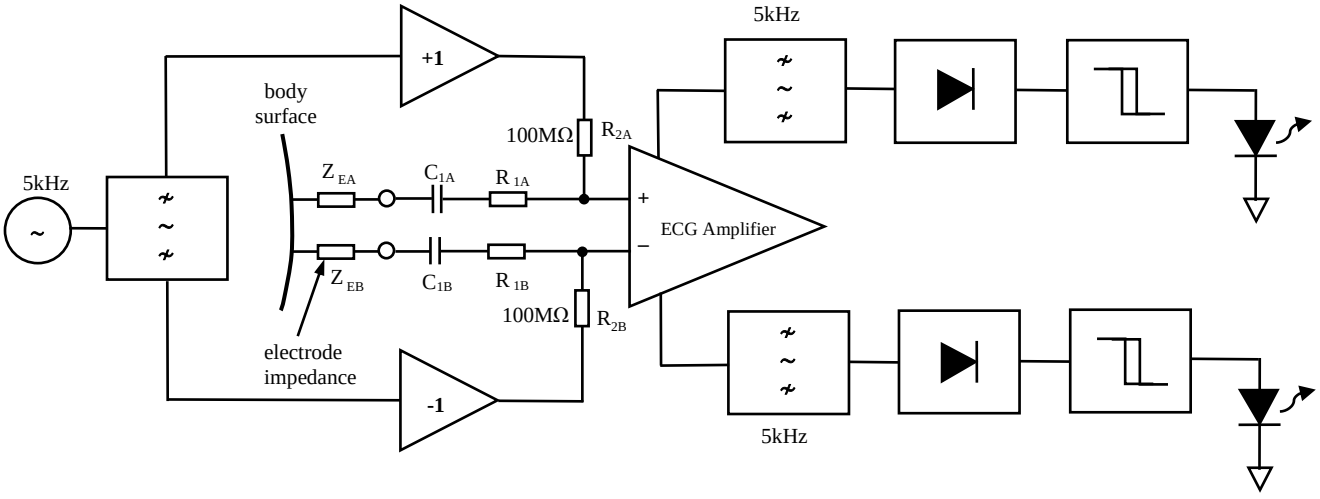

Fig.6 Block diagram of the electrode contact monitoring system

and Z_{EB}, in series with the protection resistors, R_{1A} and R_{1B}. However, there are also additional shunting capacitances present at each of the amplifier input terminals as shown in Fig.7. There is the capacitance used for rf suppression, C_{15}, which has a value of 22pF, the junction capacitance of the protection diodes, C_{diode}, which is only 0.6pF and the common-mode input capacitance of the op-amp, C_{in}, which is 6pF. These appear in parallel with the protection resistor, R_1 which is in series with the dc blocking capacitor, C_1, and the electrode impedance, Z_E. When the impedances of all of these components at the measurement frequency of 5kHz are evaluated, a simplified equivalent model of the scenario at each amplifier input terminal can be represented as shown in Fig.8. Essentially, the electrode contact impedance forms one element in a potential divider network of the various impedances shown, driven by the injected 5kHz signal at each side of the amplifier. In the case of good electrode contact, most of the 5kHz signal present is developed across the protection resistor, R_1 in each

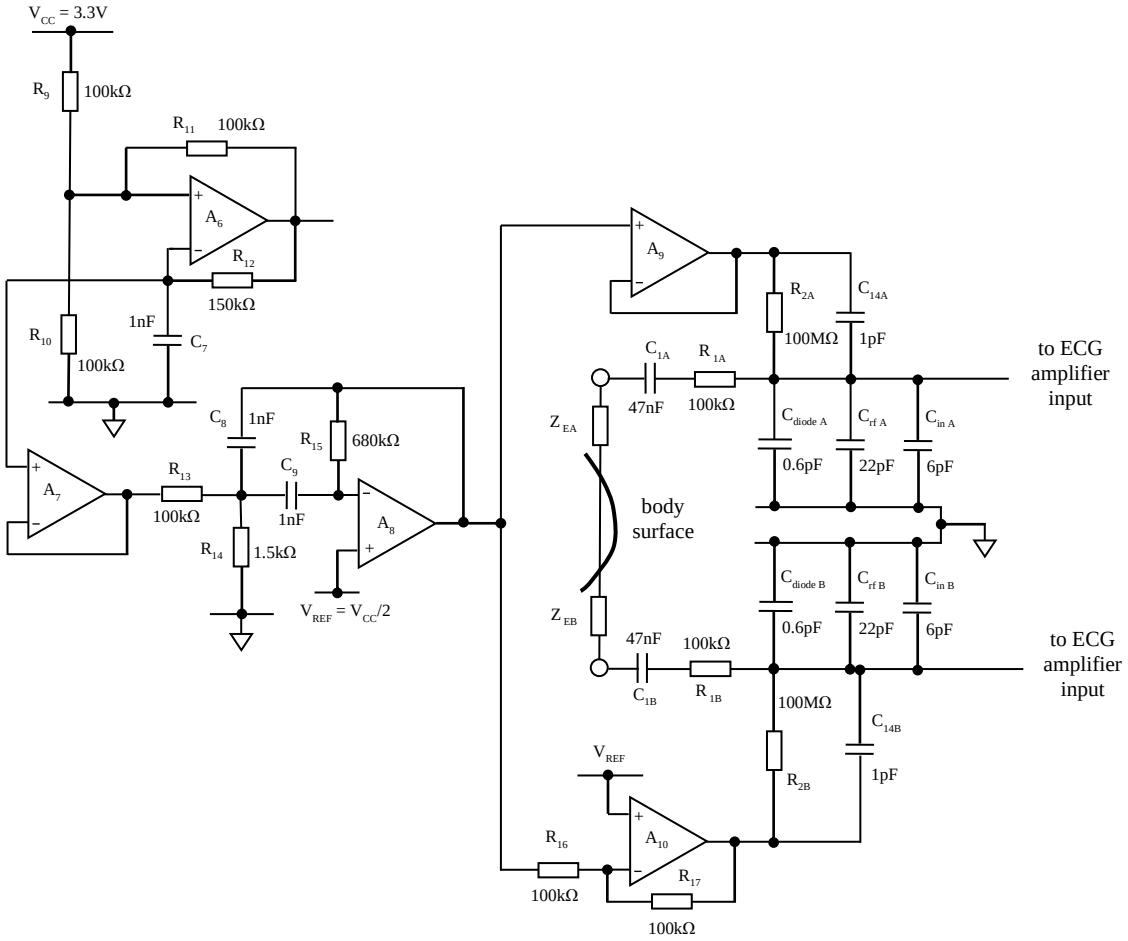

Fig.7 Schematic diagram of the signal generation and injection circuitry

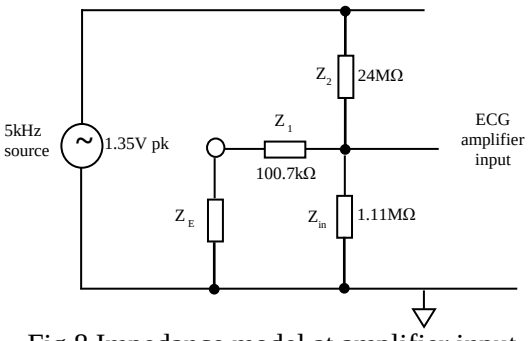

Fig.8 Impedance model at amplifier input

case. This has a value of 100kΩ, which is much greater than good quality electrode contact impedance of around 10kΩ and results in a signal level 5.6mV peak at the amplifier input. In the case of an open-circuit or disconnected electrode the maximum input signal level is 60mV. If the maximum acceptable electrode contact impedance is taken as 100kΩ as suggested by the plots of Fig.5, the expected signal level at the limit of good electrode contact appearing at the amplifier input is 10.2mVpk.

3.3 Signal extraction

It was decided to use the front-end stage of the ECG amplifier to provide the first phase of amplification for the contact monitoring signal. To this end the gains of the three stages of this amplifier were revised so that the first stage gain was modified to 23.3dB and second stage gain was revised to 24.8dB while the third stage has unity gain. The revised component values set the 3dB lower cut-off frequency of the individual differential stages at 0.34Hz which gives an overall lower 3dB cut-off frequency for the ECG amplifier of 0.53Hz, which is comfortably below the minimum value of 0.67Hz required by the international standards for clinical heart-rate monitoring.

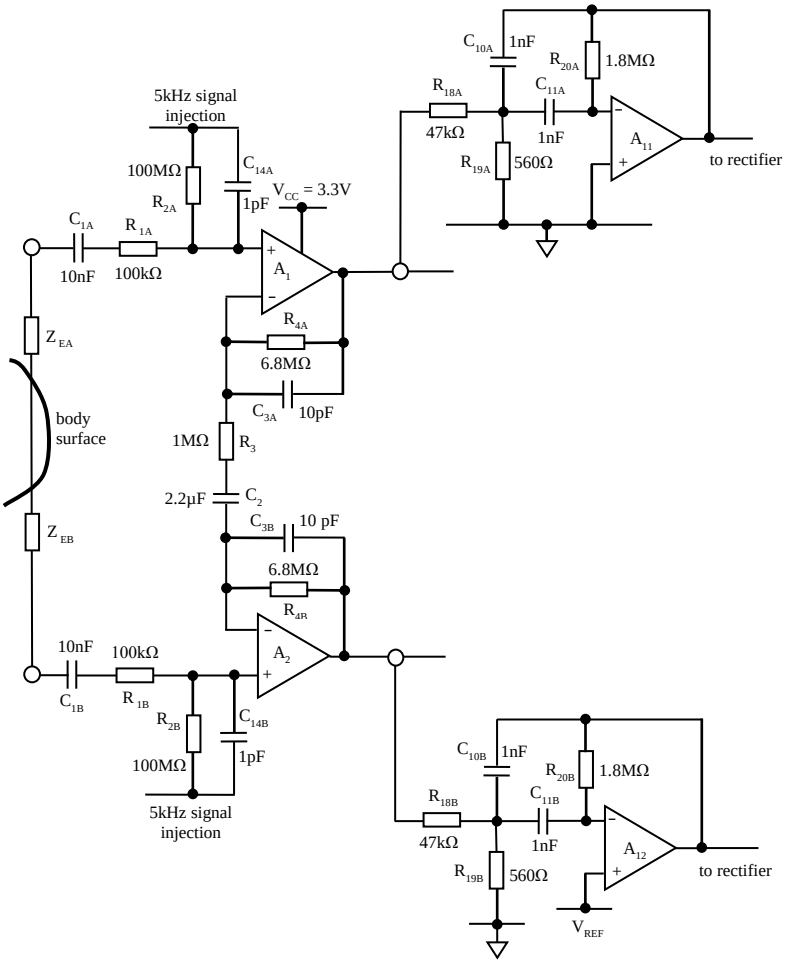

Fig.9 Schematic diagram of the signal extraction circuitry

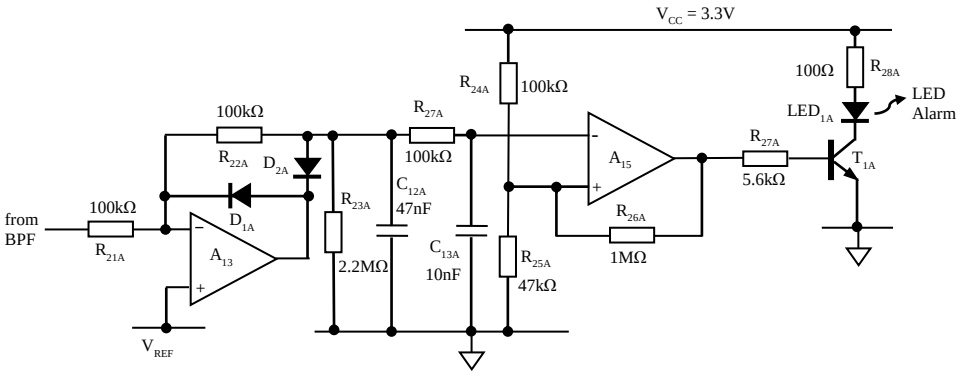

Fig.10 Schematic diagram of the rectification and threshold detection circuitry

The use of unity gain in the output differential-to-single-ended conversion stage also increases the CMRR of the ECG amplifier by 6dB. The upper 3dB cut-off frequency of the first stage was set to 10kHz while those of the second and third stages are 250Hz. A schematic diagram of the signal extraction circuitry is shown in Fig.9. The electrode contact monitoring signals are extracted from the outputs of each side of the first stage of the ECG amplifier using band-pass filters built around op-amps A_{11} and A_{12}. These filters are multiple-feedback structures having a centre frequency of 5kHz, a gain of 5 (14dB) at this frequency and a Q-factor of 11. This provides an overall gain of 61 (36dB) to the signal developed across the resistor R_1 and the electrode impedance Z_E in series. The output signal level from the filters with good electrode contact is of therefore of the order of 340mV. At the boundary of poor electrode contact impedance of 100kΩ, this rises to approximately 625mV peak.

3.4 Signal rectification and detection

A schematic diagram showing the rectification and threshold detector circuitry is given in Fig.10. The output sinewave from the band-pass filter is fed into a precision half-wave rectifier in each channel built around op-amps A_{13} and A_{14}. The rectification process is inverting and therefore provides envelope detection of the negative-going half cycles of the sinewave which is centred around the mid-supply voltage of 1.65V. The envelope voltage is maintained by means of the charge storage circuit composed of resistor R_{23} and capacitor C_{12}, having a time-constant of 0.1s. Further smoothing to remove the residual 5kHz ripple component is accomplished by resistor R_{27} and capacitor C_{13}. This provides a steady-state voltage level representing the amplitude of the recovered sinewave at 5kHz. The rectified level is negative-going with respect to the mid-supply reference voltage, V_{REF} = 1.65V. At the limit of poor electrode contact impedance, the output voltage of op-amp A_{13} or A_{14} falls to 1.025V relative to ground. This ensures an adequate voltage margin for the conduction of diodes D_1 and D_2 in the rectifier, which is therefore able to operate in a linear fashion over more than the full range of acceptable electrode contact impedance. Finally, the rectified voltages in each channel are fed into threshold detectors built around op-amps A_{15} and A_{16}. The reference voltage of each threshold detector is set at 1.022V relative to ground by resistors R_{24} and R_{25} with approximately 50mV of hysteresis added by the positive feedback provided by resistor R_{26}. This is very close to the desired threshold voltage and will give a limit of acceptable contact impedance very close to the intended value of 100kΩ. The action of the threshold detectors is inverting. Consequently, when the rectified 5kHz signal level reaches the threshold voltage, the op-amp acting as a comparator changes state and its output goes from 0V associated with good electrode contact, to the supply voltage of 3.3V associated with poor electrode contact. This HI output voltage of the op-amp is then used to feed a bipolar transistor based light-emitting-diode (LED) driver that provides a current of 2 mA to the activated LED. This level of current provides sufficient contrast of the light level to allow clear observation of the ON/OFF state of the LED.

3.5 Low power requirements

A main priority in the redesign of the electrode contact impedance monitor was to minimize the overall power consumption compared with the earlier design. The earlier design used the AD8648 which has a quiescent current of 2mA per op-amp and all of its important parameters were more than adequate for purpose. With 16 op-amps in the design this gave a current drawn from a 3.3V supply of 32mA meaning a power consumption of 105mW. This was not a concern in the initial design as it operated from a mains-driven supply. The revised version of the contact impedance monitor is expected to operate from a 3.3V battery supply with as long a lifetime as can be obtained. In order to minimize the power consumption without sacrificing performance it was necessary to use four different types of operational amplifiers. The first was the TLV3201, which is essentially a comparator with a very high slew rate and rail-to-rail operation at a quiescent current of only 40μA. This was needed to obtain accuracy in the oscillator frequency generated by the astable multivibrator. The second was the OPA345 op-amp with a gain- bandwidth product of 3MHz at a quiescent current of 50μA. This high gain-bandwidth product was needed in the bandpass filters in order to guarantee an accurate centre frequency, Q-factor and mid-band gain with minimum deviation from the design values. These were obtained in single op-amp packages as only three were needed.

The second op-amp used was the OPA4347 which had a lower gain-bandwidth product of 350kHz and a quiescent current of 20μA. This was used in the large signal buffers which needed reasonable slew-rate and the first stage of the ECG amplifier which had a bandwidth of 10kHz. A quad package was available for this op-amp so that eight of them occupied only two chips. The final op-amp was the OPA4379 which had a low gain-bandwidth product

of only 90kHz but had a very low quiescent current of only 3μA and was also available in a quad package. A 4th-order Butterworth low-pass filter with a cut-off frequency of 40Hz was also included on the board but is omitted from the schematic diagram of Fig.11. This also used the low-power OPA4379 op-amp. The important properties of each of the devices used with respect to power consumption and the performance parameters required are summarised in Table 2.

Table 2 Parameters of low-power op-amps used

Parameter	TLV3201	OPA345	OPA4347	OPA4379	Units
Gain-Bandwidth Product	-	3000	350	90	kHz
Input Impedance	10^4	10^4	10^4	10^4	GΩ
Slew Rate	500	0.8	0.17	0.03	V/μs
CMRR @ 50Hz	-	76	80	90	dB
Noise Voltage (ptp)	-	8	12	2.8	μV
Bias Current	10	10	5	5	pA
Quiescent Current	40	50	20	3	μA

4 Performance simulation

A schematic diagram showing the entire ECG amplifier and electrode contact monitoring circuit is given in Fig.11. Operation of the electrode contact monitoring system was simulated using MultiSim (National Instruments Corp.). The entire schematic of Fig.11 was entered into the schematic editor for simulation.

4.1 Contact monitoring performance

In the first instance the electrodes were modelled as pure resistors. The values of the resistors were varied in non-uniform steps from 1kΩ to 10MΩ and the signal level at the output of the filters, V_{A11}, V_{A12}, the half-wave rectifiers, V_{R23A}, V_{R23B} and the threshold detectors, V_{A15}, V_{A16}, were monitored in both upper and lower channels. These levels are shown in Table 3 and can be seen to be a little lower than the design values which is considered to be due to the loading effect of op-amp input capacitance. It can also be seen that the threshold detector logic outputs, change state at a value of electrode resistance just under 100 kΩ which is considered acceptable. This can be adjusted in the final design by including an additional resistor in parallel with the resistor R_{25} in the threshold detector and making the latter slightly larger. This will allow precise control of the critical value of electrode contact resistance which activates the LED if required.

As a more practical test, a set of electrode models identical to that of Fig.4 were created from a selection of the component values established during the tests outlined in Section 2.2. A set of 24 electrode models with different component values is given in Table 3. All of the electrode models have good electrode contact as indicated by the output logic states of the threshold detectors. The resistors R_{EA} and R_{EB} are the values of additional resistance which needed to be added in series with the electrode components in order to cause the respective threshold detectors to change state and activate the LEDs. These values range from a minimum of 80kΩ to a maximum of 110kΩ with the vast majority needing the design value of 100kΩ. The values of these resistors were established independently for the two channels, indicating that they are closely matched. The waveforms which are shown in Fig.12 illustrate the output voltage from a bandpass filter and the envelope voltage obtained at the output of the corresponding rectifier. It also shows the reference voltage and the output voltage of the associated threshold detector. The step-like nature of the waveforms can be appreciated as the circuit responds to a stepped increase in the electrode impedance covering the same range of values as in Table 3. The output voltage of the threshold detector changes state when the electrode impedance is increased from 50kΩ to 100kΩ. The actual critical value is, however, very close to 100kΩ. At impedance values above 500kΩ the outputs of these stages saturate.

Monte Carlo simulations were carried out to establish the extent of the variations in important circuit properties such as the resonant frequency and the Q-factor of the band-pass filters, under the influence of manufacturing tolerances of the components.

Table 3 Signal levels vs electrode resistance

$\|Z_E\|$	V_{A11} (Vpk)	V_{A12} (Vpk)	V_{R23A} (Vdc)	V_{R23B} (Vdc)	V_{A15} (logic)	V_{A16} (logic)
1 kΩ	0.516	0.516	1.14	1.14	LO	LO
2 kΩ	0.522	0.522	1.14	1.14	LO	LO
5 kΩ	0.541	0.541	1.12	1.12	LO	LO
10 kΩ	0.565	0.565	1.10	1.10	LO	LO
20 kΩ	0.618	0.618	1.05	1.05	LO	LO
50 kΩ	0.775	0.775	0.89	0.89	LO	LO
100 kΩ	1.038	1.038	0.64	0.64	HI	HI
200 kΩ	1.554	1.554	0.53	0.53	HI	HI
500 kΩ	1.65	1.65	0.53	0.53	HI	HI
1 MΩ	1.65	1.63	0.53	0.53	HI	HI
2 MΩ	1.65	1.65	0.53	0.53	HI	HI
5 MΩ	1.65	1.65	0.53	0.53	HI	HI
10 MΩ	1.65	1.65	0.53	0.53	HI	HI

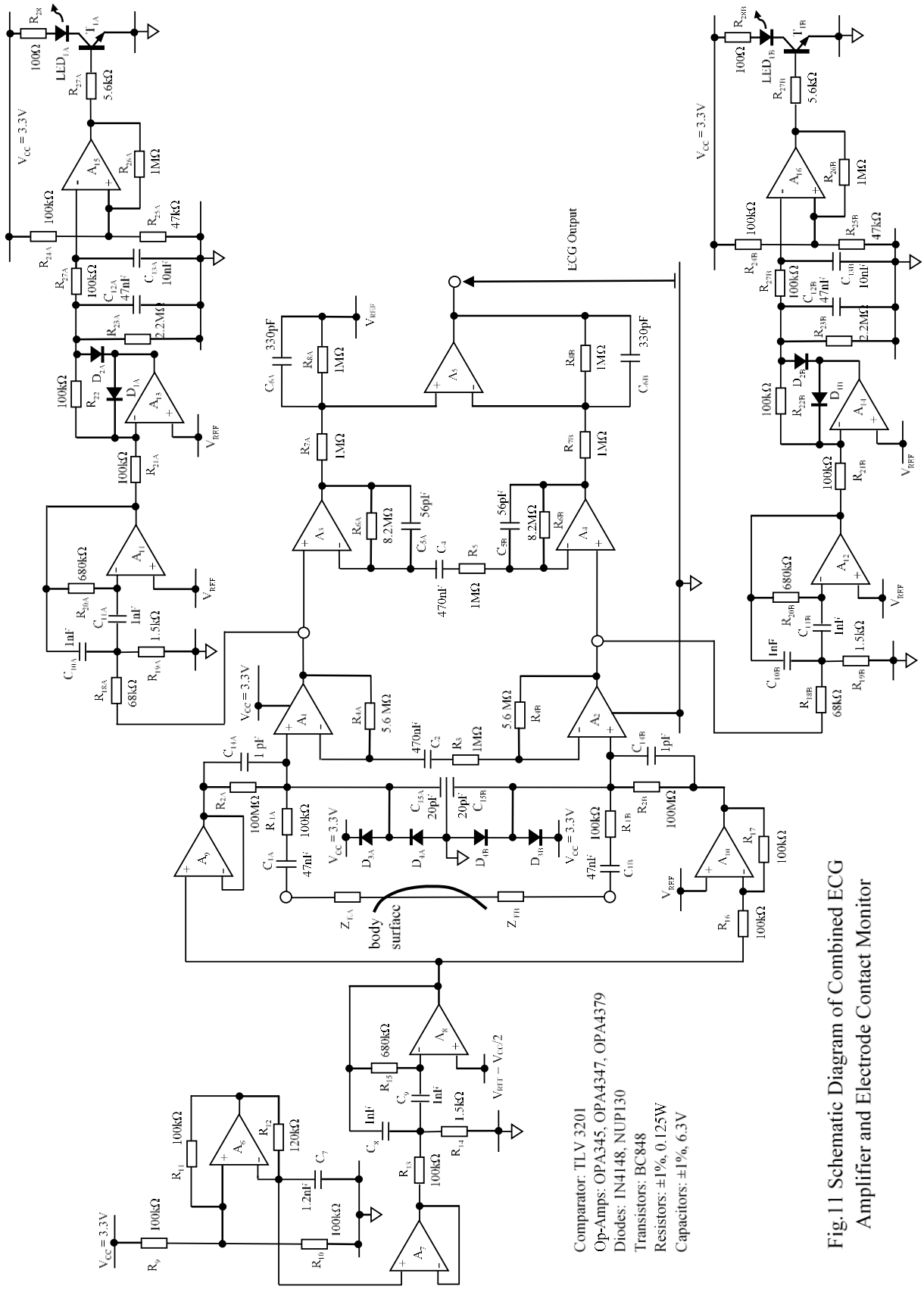

Fig.11 Schematic Diagram of Combined ECG Amplifier and Electrode Contact Monitor

Table 4 Values of signal levels recorded for a range of electrode models

No	R_1+R_3 (kΩ)	R_2 (kΩ)	C_2 (µF)	τ_2 (s)	R_4 (kΩ)	C_4 (µF)	τ_4 (s)	V_{A11} (mVpk)	V_{A12} (mVpk)	V_{R23A} (Vdc)	V_{R23B} (Vdc)	V_{A15} (logic)	V_{A16} (logic)	R_{EA} (kΩ)	R_{EB} (kΩ)
1	5	97.0	203	19.7	235	1.98	0.47	0.542	0.542	1.12	1.12	LO	LO	100	100
2	5	94.3	383	36.1	213	1.56	0.33	0.531	0.531	1.12	1.12	LO	LO	110	110
3	4	81.6	164	13.4	83.4	10.9	0.91	0.537	0.537	1.13	1.13	LO	LO	100	100
4	4	95.4	464	42.6	81.3	18.8	1.53	0.531	0.531	1.13	1.13	LO	LO	100	100
5	2	94.3	172	16.2	41.8	11.3	0.47	0.521	0.521	1.13	1.13	LO	LO	100	100
6	2	101	277	28.1	46.5	7.0	0.33	0.517	0.517	1.15	1.15	LO	LO	100	100
7	5	198	84.7	0.17	219	1.85	0.41	0.539	0.539	1.13	1.13	LO	LO	100	100
8	5	104	270	28.1	355	1.49	0.53	0.539	0.539	1.13	1.13	LO	LO	80	80
9	4	93.6	254	23.8	63.7	17.7	1.13	0.530	0.530	1.13	1.13	LO	LO	100	100
10	4	106	470	49.8	63.7	21.9	1.40	0.536	0.536	1.13	1.13	LO	LO	100	100
11	2	111	10.5	11.7	43.3	7.51	0.33	0.513	0.513	1.15	1.15	LO	LO	100	100
12	2	111	217	24.1	46.8	7.50	0.35	0.523	0.523	1.14	1.14	LO	LO	100	100
13	5	59.3	116	6.9	132	20.3	2.67	0.537	0.537	1.13	1.13	LO	LO	100	100
14	5	55.7	336	18.7	162	2.36	0.38	0.530	0.530	1.13	1.13	LO	LO	100	100
15	4	79.1	381	30.1	142	6.27	0.89	0.534	0.534	1.13	1.13	LO	LO	100	100
16	4	45.3	576	26.1	124	4.96	0.62	0.529	0.529	1.13	1.13	LO	LO	100	100
17	2	44.5	541	24.1	43.2	6.39	0.28	0.534	0.534	1.13	1.13	LO	LO	100	100
18	2	32.1	784	25.2	61.4	6.29	0.39	0.525	0.525	1.15	1.15	LO	LO	100	100
19	5	144	116	16.7	247	1.49	0.37	0.544	0.544	1.11	1.11	LO	LO	100	100
20	5	67.8	201	13.6	227	2.21	0.50	0.529	0.529	1.12	1.12	LO	LO	100	100
21	4	41.6	504	21.0	64.8	8.2	0.53	0.536	0.536	1.13	1.13	LO	LO	100	100
22	4	42.3	590	24.9	66.8	11.0	0.74	0.530	0.530	1.13	1.13	LO	LO	100	100
23	2	43.8	753	33.0	50.7	14.5	0.74	0.529	0.529	1.14	1.14	LO	LO	100	100

Table 5 Variation in circuit parameters with component manufacturing tolerances

Ocillator		Band-Pass Filter 1				ECG Amplifier	Band-Pass Filter 2				Threshold Detector
f_0	A_0	f_0	H_0	Q	BW	G	f_0	H_0	Q	BW	V_{TH}
±1.62%	±0.78%	±1.02%	±1.64%	±0.68%	±1.15%	±1.07%	±1.06%	±1.46%	±0.77%	±1.41%	±1.28%

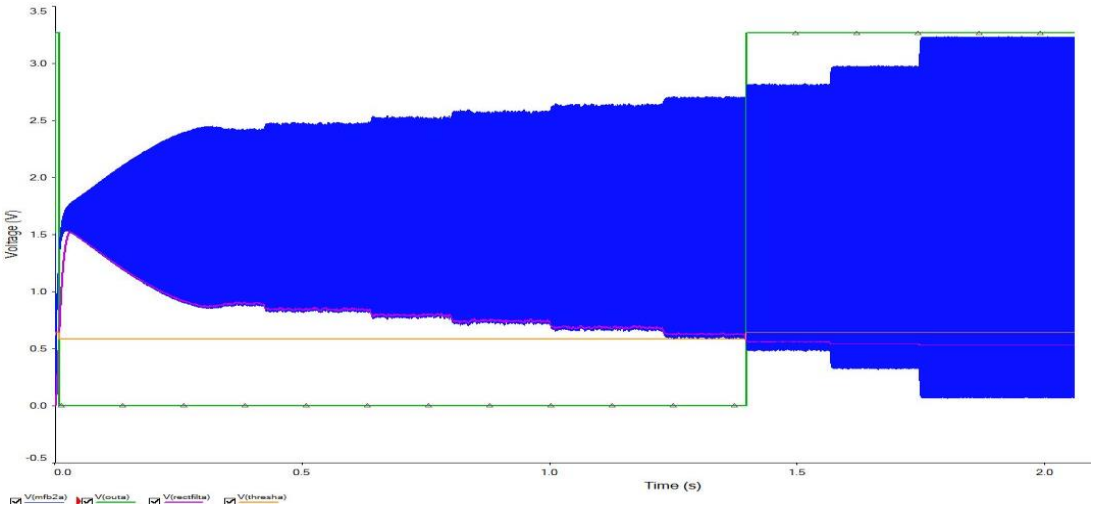

Fig.12 Waveforms showing operation of the band-pass filter, rectifier and threshold detector circuit

Table 4 shows the extremes of variation of a selection of parameters of the circuits within the electrode impedance measuring path as well as of the ECG amplifier for 500 Monte Carlo iterations. The cumulative effect of these variations affecting any single property was within ±4%, which is considered acceptable.

4.2 ECG amplifier performance

Following the design modifications made to the ECG amplifier it was also simulated to ensure that its performance had not deteriorated and still met requirements. Plots of the gain and phase vs. frequency responses of the ECG amplifier are shown in Fig.13. The mid-band gain can be seen to be 52dB in the plot, but this is because the output voltage was taken relative to only one of the differential input sources and consequently appears 6dB higher than the correct value of 46dB. The lower cut-off frequency is estimated at 0.25Hz which is well below the minimum of 0.67Hz required by performance standards. The plots also include the response of a subsequent 4th-order Butterworth low-pass filter having a cut-off frequency of 40Hz, which is evident from the plot.

The common-mode rejection ratio of the simulated circuit was also obtained and is shown in Fig.14. The plot shows a mid-band CMRR of over 90dB. It should be noted that the plot shown was obtained without mismatch in the passive components in the circuit and is consequently mainly limited by the finite CMRR of the op-amps.

Waveforms showing the output voltage at each stage of the ECG amplifier and the subsequent filter are shown in Fig.15 for steady-state conditions. The lower level signal on the lower trace is the output signal of the first stage of the amplifier, measured differentially to allow it to be observed. This illustrates the low-level input ECG signal combined with the injected 5kHz signal, where the electrode contact impedance is low corresponding to good quality of contact. The second signal on the lower trace is the output signal from the second stage of the ECG amplifier, again measured differentially for observation. It can be seen that the ECG signal has been amplified considerably in this stage, while the 5 kHz signal has been slightly attenuated. The signal on the upper trace, of Fig.15 which appears earlier in time, is the output of the 3rd differential-to-single ended conversion stage of the amplifier, having unity gain. This can be seen to be the amplified ECG signal with the 5 kHz signal entirely removed. The final signal on the upper trace, appearing later in time, is the output of the 4th order Butterworth low-pass filter. Despite the low value of cut-off frequency of 40Hz, the ECG signal appears virtually undistorted with a slight delay which does not introduce any error into the measured heart rate in the Moyo unit.

The final waveforms shown in Fig.16 are those of the output voltage of the final stage of the ECG amplifier and that of the low-pass filter, illustrating the transient conditions which prevail immediately after power-up. It can be seen that bias levels become stable within 3 seconds and that the ECG signal is available almost immediately.

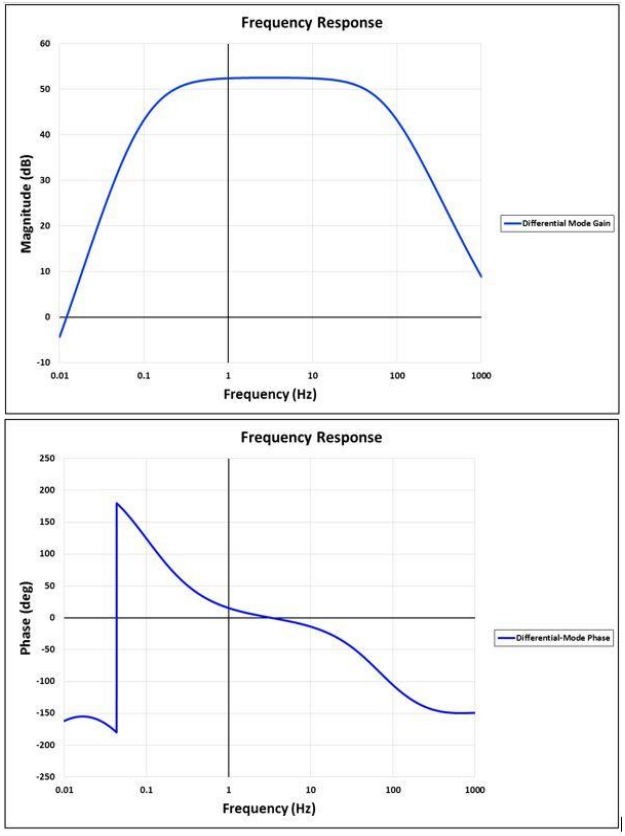

Fig.13 ECG amplifier gain and phase vs frequency

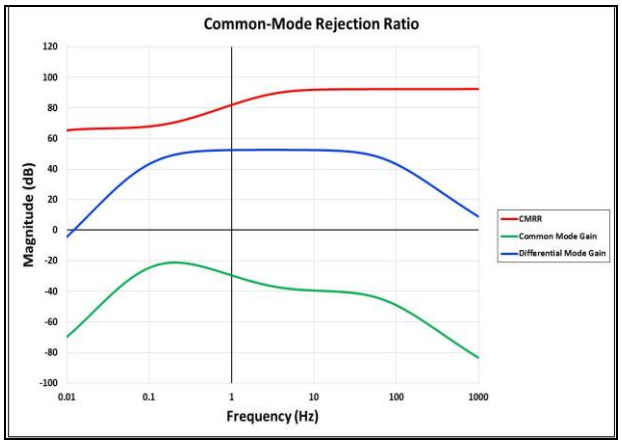

Fig. 14 Common-mode rejection vs frequency

5 Prototype evaluation

A double sided printed circuit board was designed using the Ultiboard (National Instruments Inc.) layout package. The layout was carried out for surface-mount packages of all components, including the discrete diodes, transistors and LEDs. The printed circuit board was then fabricated with a solder resistive coating and a silk screen of the component locations. Fig.17 shows the track layout of the prototype while Fig.18 presents a photo of the populated fabricated board. Three of the components had to be fitted in discrete form due to the unavailability of the surface-mount versions within a suitable time-frame. A series of bench tests was carried out on the fabricated prototype to verify its functionality and performance. The bench tests were largely the same as those applied during simulation. Table 6 and Table 7 give the voltages measured at key points in the circuit for a small range of electrode resistance values. Table 6 gives these voltages when the test electrode resistors are connected together but left floating while Table 7 shows the same voltages when the test electrode resistors are connected together and to ground. The contact impedance value at which the LEDs were illuminated proved to be a little above 100kΩ. The values are reasonably close in both cases indicating that the impedance of the patient's body has little effect on the measurement of the electrode impedance.

The performance of the ECG amplifier was also tested. Fig.19 shows a plot of the Common Mode Rejection Ratio as measured in the prototype board. This is satisfactory as it is above the 60dB required throughout the ECG amplifier bandwidth. The differential gain can be seen in the same plot and proved to provide a satisfactory frequency response.

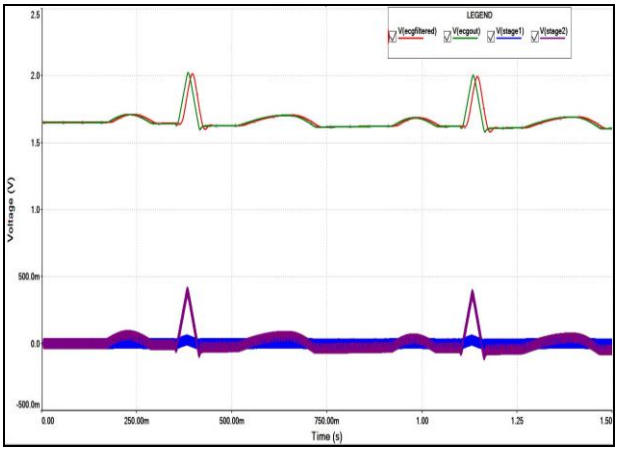

Fig.15 Output signal voltages of the amplifier

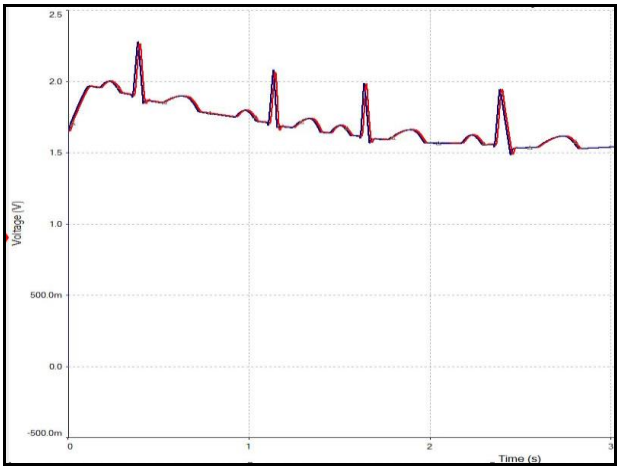

Fig.16 Output voltages following power-up

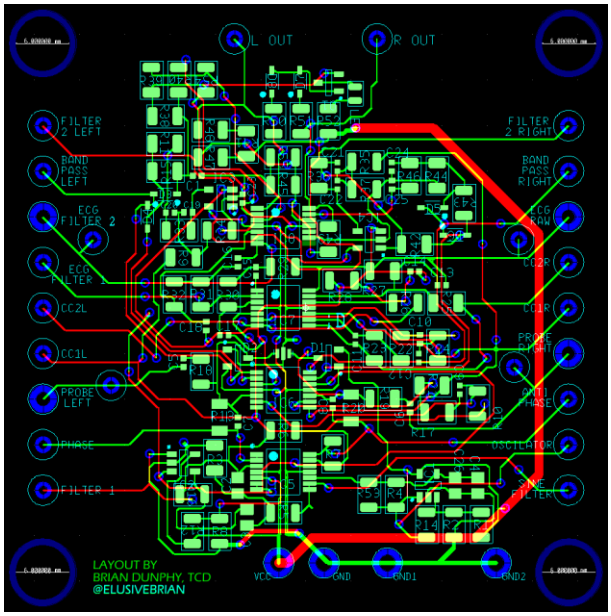

Fig.17 Track layout of the prototype

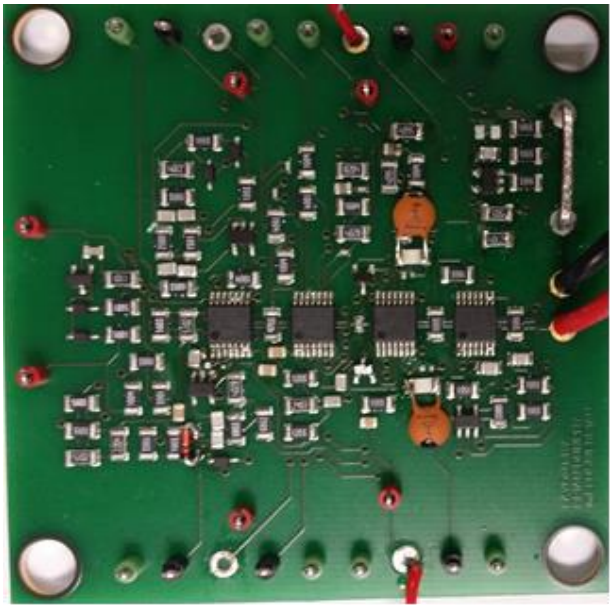

Fig.18 Populated prototype board

Table 6 Prototype voltages with Z_E floating

$\|Z_E\|$	V_{inA} (mVpp)	V_{inB} (mVpp)	V_{A1} (mVpp)	V_{A2} (mVpp)	V_{A11} (Vpp)	V_{A12} (Vpp)	V_{R23A} (Vdc)	V_{R23B} (Vdc)	V_{A15} (logic)	V_{A16} (logic)
10kΩ	26	22	166	112	0.63	0.58	1.40	1.38	LO	LO
100kΩ	40	25	285	226	0.88	0.81	1.24	1.27	LO	LO
200kΩ	50	38	380	290	1.21	1.04	1.07	1.16	HI	HI
10MΩ	64	54	608	588	2.68	2.12	0.51	0.73	HI	HI

Table 7 Prototype voltages with Z_E grounded

$\|Z_E\|$	V_{inA} (mVpp)	V_{inB} (mVpp)	V_{A1} (mVpp)	V_{A2} (mVpp)	V_{A11} (Vpp)	V_{A12} (Vpp)	V_{R23A} (Vdc)	V_{R23B} (Vdc)	V_{A15} (logic)	V_{A16} (logic)
10kΩ	14	17	108	156	0.62	0.53	1.42	1.37	LO	LO
100kΩ	35	18	228	223	0.84	0.82	1.27	1.25	LO	LO
200kΩ	48	26	340	306	1.14	1.10	1.11	1.13	HI	HI
10MΩ	64	54	612	588	2.62	2.02	0.51	0.73	HI	HI

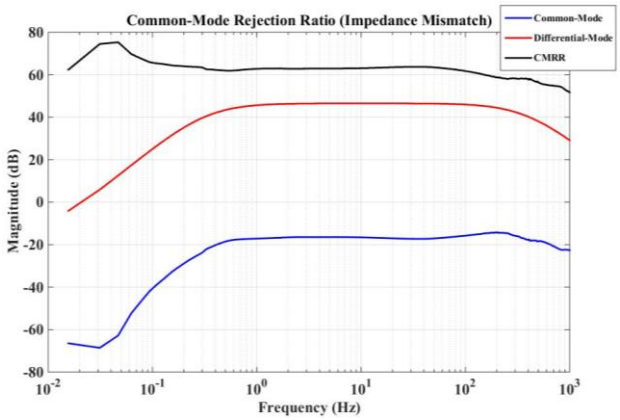

Fig.19 Common-mode-rejection-ratio of prototype

6 Conclusion

The results presented above verify the functionality of the circuit design of the electrode contact impedance monitor. In vivo use suggests that some fine tuning of the threshold detector circuit may be required to bring the design to perfection. It may be necessary to include a means of adjusting the threshold voltage of the circuit in use. It is intended that the low-power electrode impedance monitoring circuit designed will be incorporated into the next generation of the Moyo unit.

References:

[1] http://www.saferbirths.com http://www.who.int/en

[2] Murray, M. M., Maternal or Fetal Heart Rate? Avoiding Intrapartum Misidentification, *J. Obstet. Gynecol. & Neonatal Nurs.*, 33, 33-104, 2004.

[3] M. J. Burke, D. T. Gleeson, An Ultra-Low-Power Preamplifier for Pasteless Electrocardiograpy, *Proc. 6th IEEE Int. Conf. Electronics, Circuits & Systems*, Cyprus, pp616 – 619, 1999.

[4] M. J. Burke, D. T. Gleeson, A Micropower Dry-electrode ECG Pre-amplifier, *IEEE Trans. Biomed. Eng.*, 47,155-162, 2000.

[5] M. J. Burke, C. Assambo, An Improved Micro-power Pre-amplifier for Dry-electrode ECG Recording, *Proc. 11th WSEAS Int. Conf. Circuits, Systems, Communications & Computers*, Crete, Paper No. 561-286, July 2007.

[6] Assambo, C., Burke, M. J., An Improved Very-Low Power Preamplifier for Use with Ungelled Electrodes in ECG Recording, *NAUN Int. J. Biol. & Biomed. Eng.*, 1, 25-35, 2007.

[7] Burke, M. J., Assambo, C., An Ultra-Low Power Dry-Electrode ECG Amplifier Having Optimized Low-Frequency Response and CMRR, *Proc. 16th WSEAS Int. Conf. Circuits, Systems, Communications & Computers*, Kos, Paper No. 68101-025, July 2012.

[8] Assambo, C., Burke, M. J., An optimized High-Impedance Amplifier for Dry-Electrode ECG Recording, *NAUN Int J. Circuits, Systems & Signal Processing*, 6, 332–341, 2012.

[9] Baba, A., Burke, M. J., Electrical Characterization of Dry Electrodes for ECG Recording, *Proc. 12th WSEAS Int. Conf. Circuits, Systems, Communications & Computers*, Crete, Paper No. 591-226, July 2008.

[10] Baba, A., Burke, M. J., Measurement of the Electrical Properties of Ungelled ECG Electrodes, *NAUN Int. J. Biol. & Biomed. Eng.*, 2, 89-97, 2008.

[11] International Eletrotechnical Commission, Medical electrical equipment Part 2-27: Particular requirements for the safety, including essential performance, of electrocardiographic monitoring equipment, *IEC Std.* IEC60601-2-27: 2011, 3rd ed., March 2011.

[12] M. J Burke, C. Molloy, H. Fossan, High-Impedance Electrode Contact Monitoring, *Proc. 19th Int. Conf. Circuits, Sys., Comm. & Comput.*, CSCC, Zakynthos, Paper No. 581-6000, July 2015.

[13] M. J. Burke, C. Molloy, H. Fossan, Contact Monitoring of Un-gelled Stainless-Steel Electrodes, *NAUN Int. J. Biol. & Biomed. Eng.*, 10, 30–39, 2016.